Nuclear Engineering and Design 272 (2014) 92–98

Contents lists available at ScienceDirect

Nuclear Engineering and Design

journal homepage: www.elsevier.com/locate/nucengdes

# The oxidation behavior of three different zones of welded Incoloy 800H alloy

W.S. Chen [a], W. Kai [a,*], L.W. Tsay [a], J.J. Kai [b]

[a] Institute of Materials Engineering, National Taiwan Ocean University, Keelung 20224, Taiwan, ROC
[b] Department of Engineering and System Science, National Tsing Hua University, Hsinchu 30050, Taiwan, ROC

## HIGHLIGHTS

- The oxidation kinetics of 800H followed the parabolic-rate law in dry-air.
- The scales formed on the alloys were composed of $Cr_2O_3$ and $MCr_2O_4$ (M = Fe, Cr).
- Internal-oxidation of $Al_2O_3$ and $SiO_2$ dissolved $T_i$ were observed in 800H-SUB and 800H-HAZ
- The weight loss behavior of 800H-SUB and 800H-HAZ were observed in wet air.
- The mass-loss behavior of 800H-HAZ is more severe than 800H-SUB in wet air.

## ARTICLE INFO

*Article history:*
Received 22 July 2013
Received in revised form 22 January 2014
Accepted 28 January 2014

## ABSTRACT

The oxidation behavior of three different zones of welded Incoloy 800H alloys, containing the substrate (800H-SUB), heat-affected zone (800H-HAZ) and the melt zone (800H-MZ) was studied at 950 °C in dry and wet air. The steady-state oxidation rate constants ($k_p$ values) were calculated based on the mass-gain data, and the oxidation resistant ability of the alloys followed by the rank of 800H-MZ > 800H-SUB > 800H-HAZ in dry air. The scales formed on the 800H-SUB and 800H-HAZ consisted of a heterophasic mixture of $Cr_2O_3$ and $FeCr_2O_4$, while a mixture of $Cr_2O_3$ and $MnCr_2O_4$ was observed on the 800H-MZ. On the other hand, the oxidation kinetics of the alloy, initially followed the parabolic-rate law up to 48 h, while a significant mass-lost kinetics was observed for a prolong exposure in wet air. The detail oxidation mechanisms for the alloys in both environments were investigated.



## 1. Introduction

Superalloys are considered for using in many power-generating facilities (Davis, 1997; Rai et al., 2004), which can be used in heat-exchange tubes of High Temperature Gas Reactor (HTGR) of nuclear-power plant (Fiorrenttin, 1987). The chemical composition of Incoloy-800H (800H) was shown in Table 1, and Ni content is more higher than stainless steel which the mechanical properties and oxidation resistance of 800H alloy become better. In general, the oxidation resistance of an alloy strongly depends on the dense nature of the scale and its good adhesion to the substrate at elevated temperatures. Typically, a chromia-former alloy with adequate amounts of Cr content (≥20 wt.%) may expect to form a full-dense, continuous $Cr_2O_3$ layer in the scales, which effectively blocks outward diffusion of cations and inward transport of oxygen, thereby providing an excellent benefit effect against further oxidation (Wood and Stoot, 1987; Cabet and Rouillard, 2009). In addition, depending on alloy composition, several Cr-containing spinels, such as $(M,Cr)_3O_4$ where M = Fe, Ni, Mn, or Ti, were always observed on top of the chromia layer (Asteman et al., 2001; Tempest and Wild, 1982; Laverde et al., 2004). The diffusivities of those cations (Fe, Mn, Ni and Ti) were much faster than those of Cr ions in the $Cr_2O_3$ sub-lattices, having the order of $D_{Mn} > D_{Fe} > D_{Ni} > D_{Cr}$ (Kim et al., 2009; Lobnig et al., 1992). Thus, the formation of various spinels may also provide a protective layer to reduce the oxidation rates.

In addition, a proper welding process is applied to assemble the parts of heat-exchangers, and it is expected that the properties of those welded alloys may significantly change. Thus, it is of essence to fully understand the welding effect on the possibility of materials degradation in the 800H alloy when applied in practical industries during thermal activated processes, especially when water vapor presents in the environments. According to various positions of heat-exchangers from the reactor, the operation

* Corresponding author. Tel.: +886 2 2462 2192x6415.
*E-mail address:* wkai@mail.ntou.edu.tw (W. Kai).

http://dx.doi.org/10.1016/j.nucengdes.2014.01.022
0029-5493/

**Table 1**
The chemical composition of Incoloy 800H and Inconel 82 alloys.

| Alloy | Element | | | | | | | | |
|---|---|---|---|---|---|---|---|---|---|
| | Ni | Cr | Fe | Al | | Mn | Co | Mo | Other |
| Incoloy 800H | 32.0 | 19.6 | 46.0 | | 0.4 | 0.8 | – | – | Cu,Ti,Si |
| Inconel 82 | 67.0 | 22.0 | 3.0 | | – | 2.5 | 0.1 | 0.5 | Si,Ti |

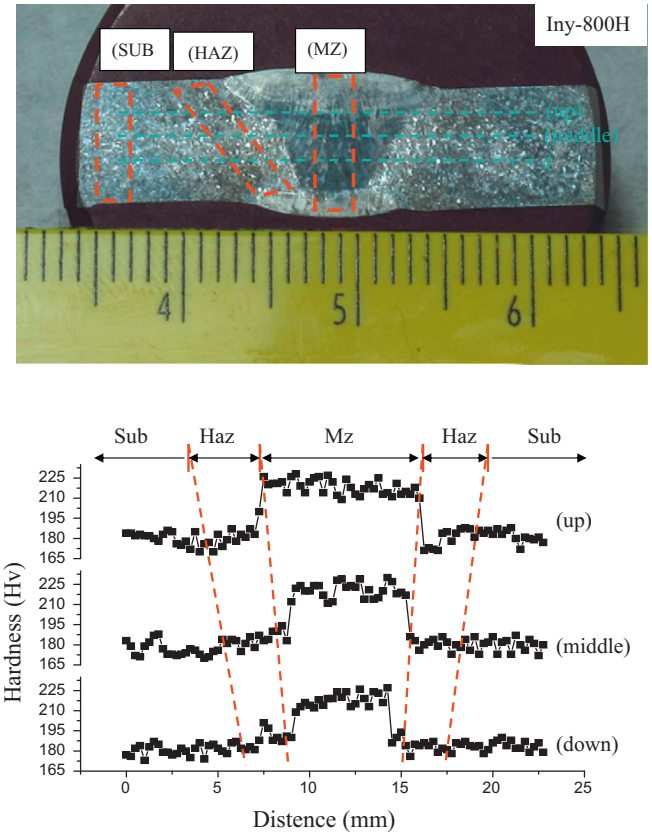


**Fig. 1.** Metallographic and hardness of the 800H after welding.

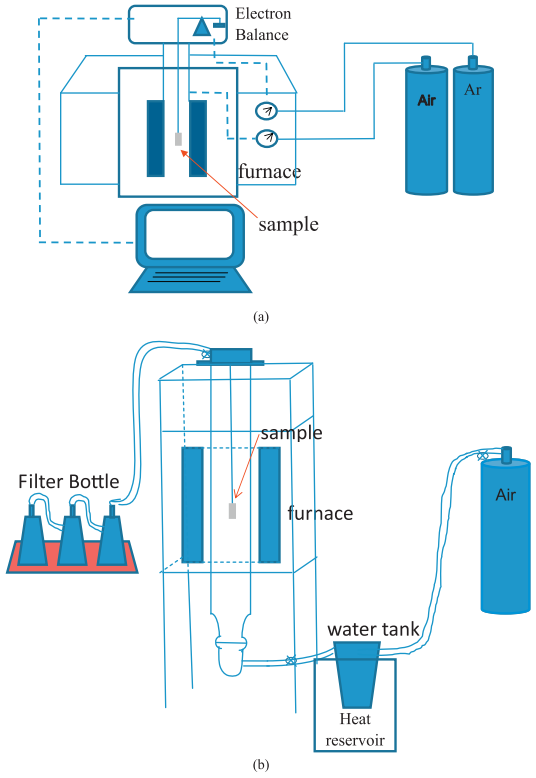


**Fig. 2.** The systems of oxidation tests (a) TGA and (b) tube furnace.

temperature could be from 950 °C at the entrance side to 390 °C at the exit side (Fujikawa et al., 2004). Thus, the main goal of this work is to systemically study the oxidation behavior of the welded 800H alloy in dry/wet air at 950 °C. The effects of welding and water vapor on oxidation kinetics and reaction mechanism of the 800H superalloy are explored.

## 2. Experimental

A commercial 800H sheet (100 cm × 60 cm × 0.6 cm) was directly purchased from the local supplier. The welding process was done by TIG under an atmosphere of Ar. Two alloy plates with V-slot of 45° were assembled, and Inconel-82 (the composition also shown in Table 1) was chosen as the filler, as suggested by AWS-A5.14 specification (AWS, 2011). The welded 800H alloy produced three different zones with after welding process were obtained three different zones, as shown in the optical micrograph and hardness measurement of Fig. 1, containing the substrate (800H-SUB), the melting zone (800H-MZ), and the heat-affected zone (800H-HAZ).

The testing samples were cut into the rectangle-shape in the red area (sample size about 1.5 cm × 1.0 cm × 0.2 cm) by a cutting machine, and grounded down to 1000 grit SiC paper. The oxidation tests of the samples were carried out by the TGA at 950 °C in dry air, as shown in Fig. 2a. The wet air (air + 50% $H_2O$) was generated by passing the dry air (with its flow rate of 400 $cm^3$/min) through a water-tank reservoir at 81.5 °C before into the tube furnace (as Fig. 2b).

After the oxidation tests, the characterization of the scale constitution and phases was analyzed using X-ray diffraction (XRD), optical microscopy (OM) and scanning electron microscopy (SEM) under back-scattered electron image (BEI) mode and energy dispersive spectrometry (EDS).

## 3. Results and discussion

### 3.1. Oxidation kinetics

Parabolic plots of oxidation kinetics for the three different zones of welded 800H alloy in dry and wet air at 950 °C are shown in Fig. 3. In general, the dry-air oxidation kinetics of the three zones of welded 800H obeyed a parabolic-rate law, having a simple mass-gain trend throughout the exposure period of time. The parabolic-rate constants ($k_p$ values) were determined by the equation of $\Delta m/A$ (mass gain per unit area) = $k_p(t)^{1/2}$ at the steady-state stage, and the calculated $k_p$ values (in the unit of $g^2/cm^4/s$) were around $8.06 \times 10^{-12}$, $1.11 \times 10^{-11}$, and $7.62 \times 10^{-12}$ for 800H-SUB, 800H-HAZ, and 800H-MZ, respectively. It is obvious that the oxidation rates of the alloys followed by the rank of 800H-HAZ > 800H-SUB > 800-MZ, and the observed steady-state parabolic kinetics further confirmed solid-state diffusion being the rate-controlling step during dry-air oxidation.

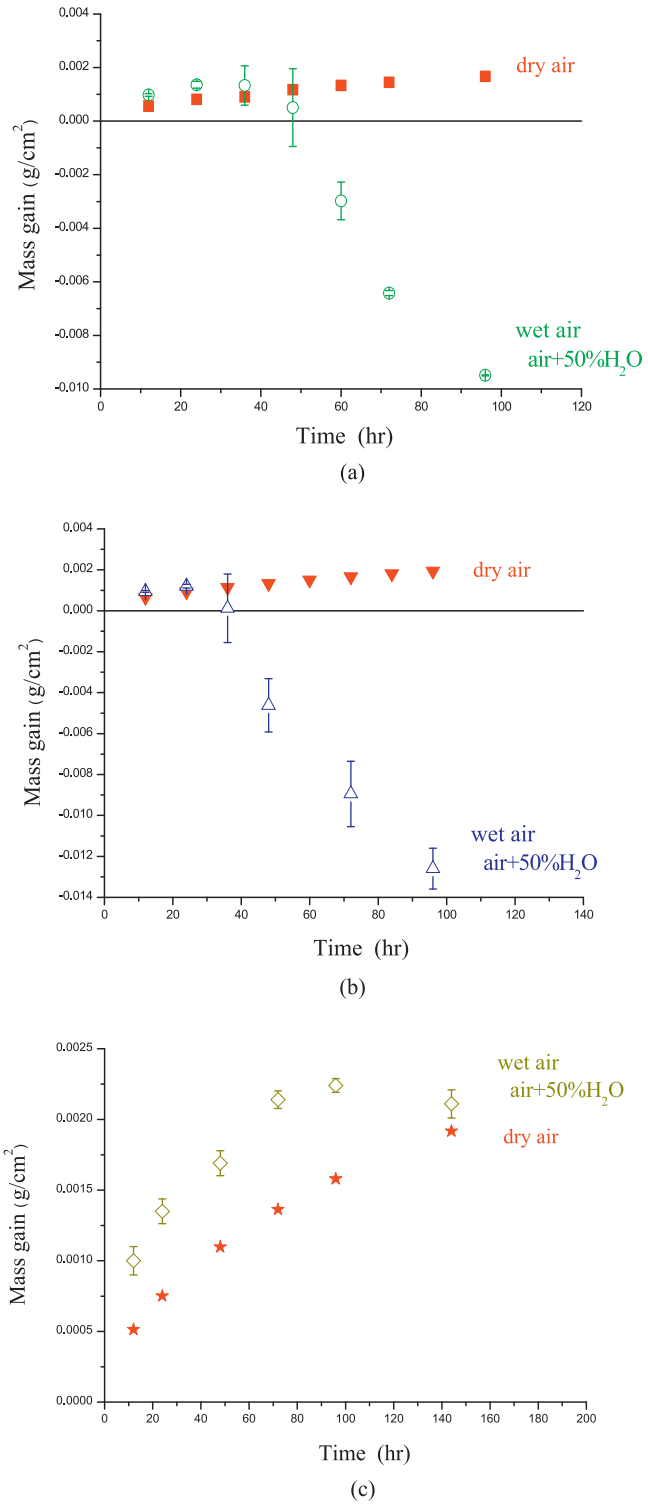


**Fig. 3.** Oxidation kinetics of (a) 800H-SUB, (b) 800H-HAZ and (c) 800H-MZ in dry/wet air at 950 °C.

On the other hand, the oxidation kinetics for the same zones of welded 800H in wet air were significantly different from those in dry air, being divided into at least two different kinetics periods, depending on exposure duration. An initial mass-gain period was observed for the alloys, indicative of a similar diffusion-controlled reaction, and then, followed by a later mass-loss period. The duration of exposure time to cause the mass loss was strongly dependent on the alloy. For example, the mass loss of 800-SUB was observed after a 48 h exposure, whereas similar mass-loss results were observed for 800H-HAZ and 800H-MZ after shorter exposure periods of time for 36 and 144 h, respectively. The observed mass-loss kinetics in wet air after a certain period of exposure time was never observed in dry-air oxidation, which could be due presumably to the instability of the scales, which in turn deserved further discussion on the scale constitution in the following section.

**Table 2**
The total scale-thickness of 800H-SUB, 800H-HAZ, and 800H-MZ oxidized in wet air at 950 °C.

| | 24 h | 48 h | 96 h |
|---|---|---|---|
| 800H-SUB | 13.7 ± 1.4 μm | 9.9 ± 0.7 μm | 7.8 ± 1.3 μm |
| 800H-HAZ | 14.2 ± 1.0 μm | 6.9 ± 0.8 μm | 6.3 ± 1.1 μm |
| 800H-MZ | 8.8 ± 0.5 μm | 11.9 ± 1.0 μm | 23.2 ± 0.9 μm |

### 3.2. Scale constitution and phases

Typical cross-sectional BEI micrographs of the scales formed on the three different zones of welded 800H alloy after oxidation for 48 h at 950 °C in dry air is shown in Fig. 4, revealing a duplex-scale nature in the alloys. All the scales remained good adherence to the substrate, which further implied a good agreement with the mass-gain oxidation-kinetics trend. In addition, XRD analyses (Fig. 4) showed that the outer layer consisted mostly of $FeCr_2O_4$ and minor $Cr_2O_3$, while an exclusively inner-layer of $Cr_2O_3$ was observed for both 800H-SUB and 800H-HAZ. On the other hand, $MnCr_2O_4$ was present but $FeCr_2O_4$ was absent in the outer-layer scale of 800H-MZ although the inner layer of $Cr_2O_3$ was identical. Note that the peak intensities between the two spinels were very close, their discrepancy was further confirmed by EDS analyses that a certain amount of Mn (~15.8 at.%) was detected in the outer scale of 800H-MZ, while Mn was absent in the same locations for the other two alloys. In addition, the average total thickness of the scales for the three zones was around 11.91 ± 0.54, 10.68 ± 0.81, and 9.19 ± 0.61 μm for 800H-HAZ, 800H-SUB, and 800H-MZ, respectively. This observation is also in good agreement with the kinetics study, having the thicker the scale thickness the higher the oxidation rate. According to the results of the oxidation kinetics and scale constitution in dry air, it is evident that the $MnCr_2O_4$ spinel grown on top of the chromia layer provides a better oxidation resistance than $FeCr_2O_4$, as similar to that reported in England and Virkar (1999).

Another interesting aspect to further discuss is that minor amounts of discontinuous precipitates were noted in the substrate just beneath the scales. EDS analyses confirmed two different internal oxides for those precipitates, consisting of larger gray-islands of $Al_2O_3$ and tiny black spots of $SiO_2$ dissolved with minor Ti for both 800H-SUB and 800H-HAZ zone. On the other hand, only $SiO_2$ were observed in 800H-MZ.

The observed internal-oxidation precipitates were due certainly to lower concentrations of those elements in the alloy substrate, which were much lower than critical concentrations to form the continuous layers under kinetic reasons, as suggested in Rapp (1965).

On the other hand, SEM micrographs and XRD analyses of the alloys oxidized in wet air are further shown in Figs. 5–7. Duplex scales were also detected in the wet-air environment; however, the thickness of the outer layer is much thinner (depending on exposure duration) while numerous pores were present in the inner layer. For example, the scales formed on 800H-SUB after the oxidation for 24, 48, and 96 h at 950 °C are shown in Fig. 5. The total scale-thickness of the three zones of welded 800H alloy were measured and are summarized in Table 2. As can be seen in Fig. 3a, the wet-air oxidation kinetics of 800H-SUB experienced a mass-loss

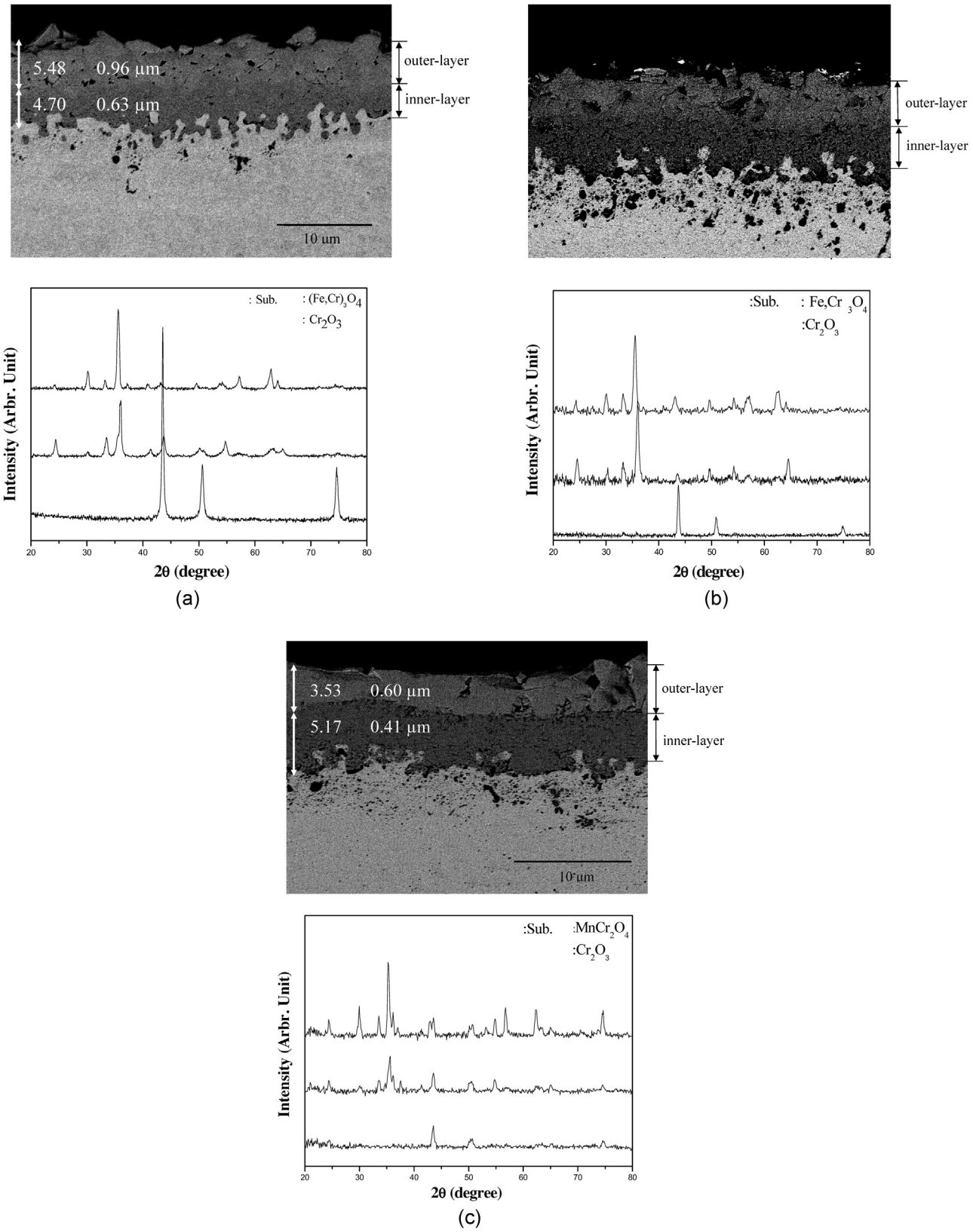


**Fig. 4.** Cross-sectional BEI micrographs and XRD analyses of the (a) 800H-SUB, (b) 800H-HAZ and (c) 800H-MZ oxidized in dry air at 950 °C for 48 h.

after the 48 h or longer exposures, so that the total scale-thickness could be slightly reduced. Its relative cross-section micrograph is further shown in Fig. 5, revealing that the outer-layer scale was peeled off in certain regions. Thus, it may be concluded that the mass-loss kinetics of 800H-SUB is due mainly to the spallation of scale.

In addition, the surface topographies of the scales formed on 800H-HAZ for various durations of time are shown in Fig. 6.

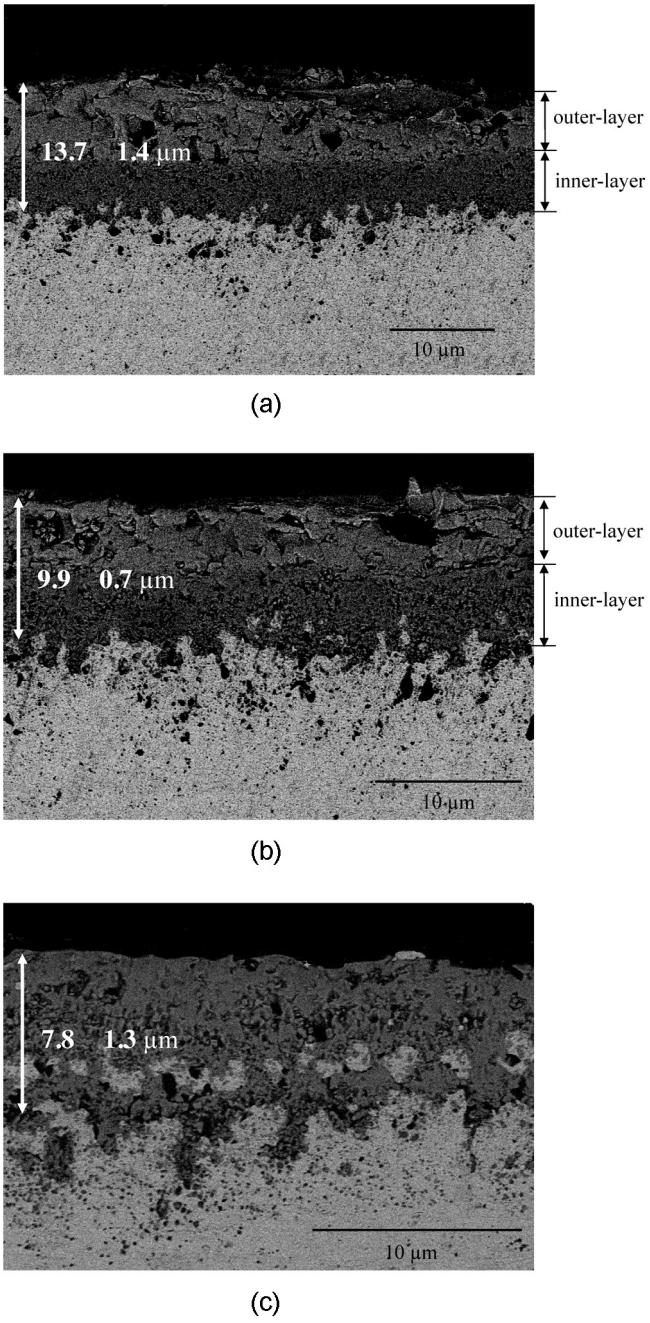


**Fig. 5.** Cross-sectional BEI micrograph of the 800H-SUB oxidized in wet air at 950 °C for (a) 24, (b) 48, and (c) 96 h.

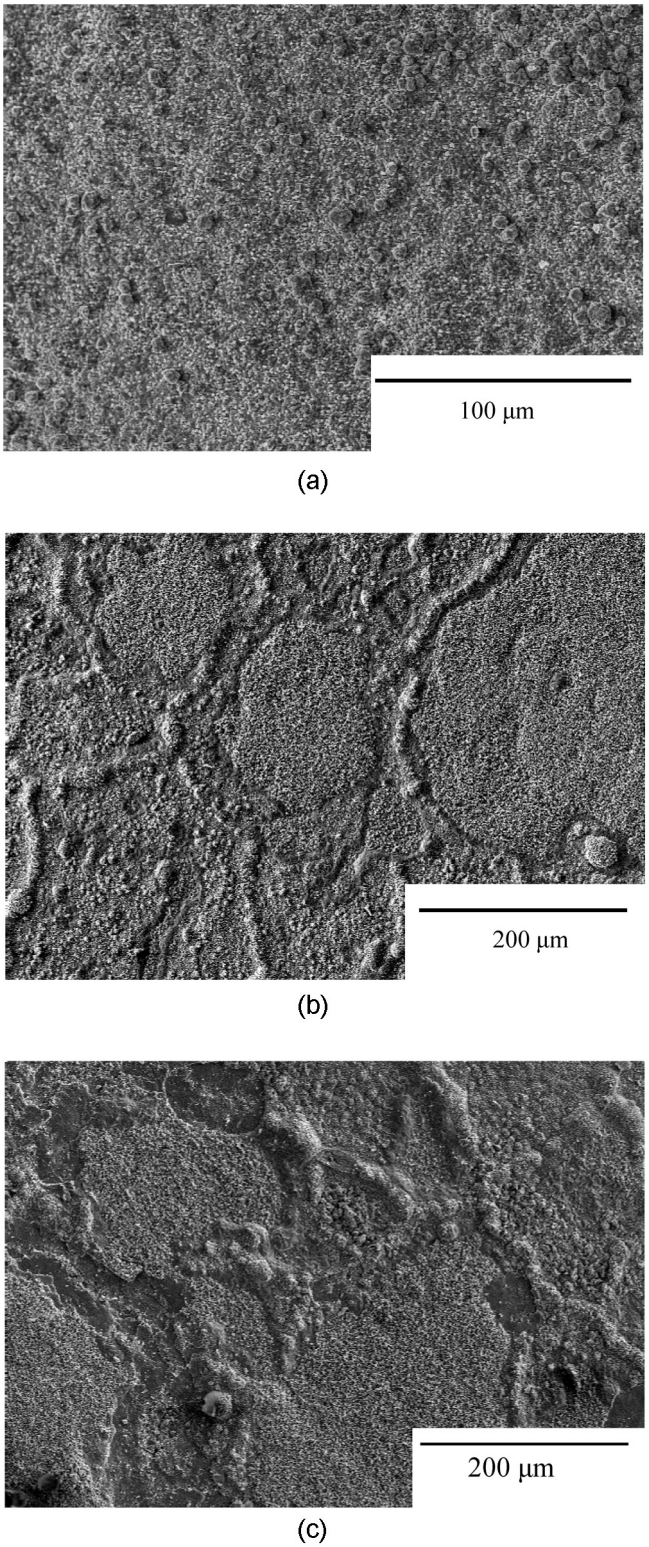


**Fig. 6.** Surface topographies of the 800H-HAZ oxidized in wet air at 950 °C for (a) 48, (b) 72, and (c) 96 h.

Although not shown here, XRD analyses revealed that mostly $(Fe,Cr)_3O_4$ spinel and minor $Fe_2O_3$ throughout the scales. The observed pores and oxide humps should be related to the mass-loss phenomenon for 800H-HAZ which deserved further discussion. The fact is that the water vapor present in the wet-air oxidation at elevated temperatures may lead to its decomposition to form both $OH^-$ and $H^+$ ions which could rapidly diffuse into the inner-/outer-scale interface or the inner-layer/substrate boundary during oxidation. Very likely, a further reduction of $H^+$ ions may form hydrogen molecules inside the scales, which in turn results in the growth stress to weaken the scale adherence, thereby leading to detaching the outer layer from the scales. Thus, the scale spallation and the formation of oxide humps observed in the wet-air oxidation of the 800H-HAZ could be responsible for the mass-loss kinetics in shorter exposure duration. Note that certain amounts of pores and cracks were observed for 800H-HAZ after a 48 h exposure in wet air, and additional oxide humps along the grain-boundary areas were also observed after longer exposures for 72 and 96 h. The reason is that Ti(C,N) and $Cr_{23}C_6$ are precipitates at the grain boundaries, so become the $O^{2-}$ ions or $OH^-$ inward diffusion easily at Cr-depleted zone.

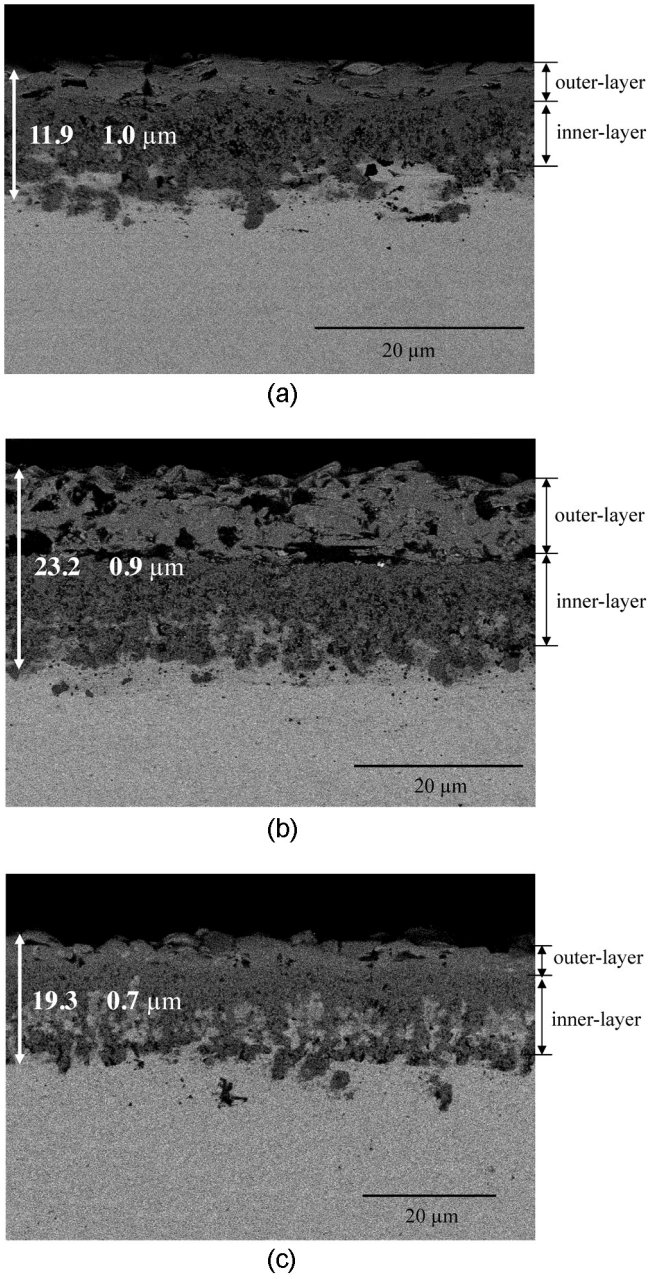


**Fig. 7.** Cross-sectional BEI micrographs of the 800H-MZ oxidized in wet air at 950 °C for (a) 48, (b) 96, and (c) 144 h.

Typical cross-sectional BEI micrographs and XRD analyses of the scales formed on 800H-MZ are shown in Fig. 7. The scales formed on this zone in wet air consisted of an intermixed layer of $MnCr_2O_4$ and $Cr_2O_3$. Yet, the exposure duration to start the mass-loss kinetics is after a time interval of 96 h for 800H-MZ, which is much longer than that of the 800H-HAZ and 800H-SUB. The observed mass-loss for the three zones indicated that the instability of the scales could be due mainly to the thermal residual stress formed on the scale/substrate boundary, as similarly discussed above. According to Tan et al. (2008), the linear coefficients of thermal expansion (CTE values) for $Fe_2O_3$, $Fe_3O_4$, and $FeCr_2O_4$ (or $MnCr_2O_4$) were about $14.9 \times 10^{-6}$, $15.2 \times 10^{-6}$, and $8.8 \times 10^{-6}$ (cm/cm K) at 950 °C, respectively, which were much higher than that of $Cr_2O_3$ ($7.3 \times 10^{-6}$ cm/cm K) but much lower than that of the substrate ($\sim 17.6 \times 10^{-6}$ cm/cm K). Very likely, the growth of the complex iron oxides or their spinels on top of chromia should generate a certain amount of tensile residual stress, which in turn may cause the peel-off scales from the outer- and inner-layer interface. In addition, the growth of chromia in the inner layer may also produce a compressive residual stress with respect to the substrate, which could also detach the whole scales from the substrate. Based on the microstructure analyses described above, it is evident that the former situation prevailed in the current study, while the later case was never observed. Furthermore, the mass-loss feature is due primarily to the thermal residual stress in wet air; yet it was not observed in dry air condition. This observation may further imply that both $H^+$ or $OH^-$ ions present in the wet-air environment could weaken the scale adherence, which eventually caused the spallation between the outer- and inner-layer scale.

## 4. Conclusions

Based on the results and research, following several conclusions can be drawn.

1. The oxidation kinetics of three different zones of welded 800H alloy followed the parabolic-rate law in dry-air oxidation, indicating that diffusion is the rate-controlling step during oxidation. The dry-air oxidation rates of the alloys followed by the fast-to-slow rank of 800H-HAZ > 800H-SUB > 800H-MZ.
2. The scales formed on the alloys were composed of $Cr_2O_3$ and $FeCr_2O_4$ for both 800H-SUB and 800H-HAZ, and $MnCr_2O_4$ for 800H-MZ. Internal-oxidation precipitates of $Al_2O_3$ and $SiO_2$ dissolved Ti just beneath the substrate were observed in 800H-SUB and 800H-HAZ, but only $SiO_2$ were observed in 800H-MZ.
3. The scales formed on the alloys in the wet-air environment were similar to those in dry air, however, their oxidation behavior experienced two different kinetics stages in wet air, consisting of an initial mass-gain stage, and then, followed by a second mass-loss stage.
4. The effects of welding on the oxidation kinetics of the 800H alloy were discussed, and it was found that the 800H-HAZ alloy oxidized much faster than 800H-SUB and 800H-MZ in dry air. In addition, the mass-loss behavior of 800H-HAZ is also more severe than that of 800H-SUB and 800-MZ in wet air.

## Acknowledgments

Partly financial support by the National Science Council of Republic of China under the Grant Nos. of 100-NU-E-019-001-NU and NSC 99-3113-Y-042-001 is greatly acknowledged. TGA equipment support by the National Taiwan Ocean University under the Grant No. of NTOU-RD972-04-03-01-01 is also appreciated.

## References

Asteman, H., Segerdahl, K., Svensson, J.E., Johansson, L.G., 2001. The influence of water vapor on the corrosion of chromia-forming steels. Mater. Sci. Forum 369, 277.
AWS A5.14/A5.14M, 2011. Specification for Nickel and Nickel-Alloy Bare Welding Electrodes and Rods.
Cabet, C., Rouillard, F., 2009. Corrosion of high temperature metallic materials in VHTR. J. Nucl. Mater. 392, 235.
Davis, J.R., 1997. Heat Resistant Materials (ASM Specialty Handbook). ASM International.
England, D.M., Virkar, A.V., 1999. Oxidation kinetics of some nickel-based superalloy foils and electronic resistance of the oxide scale formed in air. Part I. J. Electrochem. Soc. 146 (9), 3196.
Fiorrenttin, S.R., 1987. Study of γ′-precipitation kinetics in alloy 800 at 575 °C by small angle neutron scattering. Nucl. Instr. Meth. Phys. Res. B B22 (4), 564.
Fujikawa, S., Hayashi, H., Nakazawa, T., Kawasaki, K., Iyoku, T., Nakagawa, S., Sakaba, N., 2004. Achievement of reactor-outlet coolant temperature of 950 °C in HTTR. J. Nucl. Sci. Technol. 41, 1245.
Kim, D., Jang, C., Ryu, W.S., 2009. Oxidation characteristics and oxide layer evolution of Alloy 617 and Haynes 230 at 900 °C and 1100 °C. Oxid. Met. 71, 271.

Laverde, D., Acebo, T.G., Castro, F., 2004. Continuous and cyclic oxidation of T91 ferritic steel under steam. Corros. Sci. 46 (3), 613.
Lobnig, R.E., Schmidt, H.P., Hennesen, K., Grabke, H.J., 1992. Diffusion of cations in chromia layers grown on iron-base alloys. Oxid. Met. 37, 81.
Rai, S.K., Kumar, A., Shankar, V., Jayakumar, T., Rao, K.B.S., Raj, B., 2004. Characterization of microstructures in Inconel 625 using X-ray diffraction peak broadening and lattice parameter measurements. Scr. Mater. 51, 59.
Rapp, R.A., 1965. Kinetics, microstructures and mechanism of internal oxidation – its effect and prevention in high temperature alloy oxidation. Corrosion 21 (12), 382.
Tan, L., Sridharan, K., Allen, T.R., 2008. Altering corrosion response via grain boundary engineering. Mater. Sci. Forum 595, 409.
Tempest, P.A., Wild, R.K., 1982. Thickness measurements of spinel and chromia layers in stainless steel oxide scales by X-ray diffractometry. Oxid. Met. 17, 345.
Wood, G.C., Stoot, F.H., 1987. Oxidation of alloys. Mater. Sci. Technol. 3, 519.